Accurate decoding of reaching movements from field potentials in the absence of spikes

2012 J. Neural Eng. 9 046006

(http://iopscience.iop.org/1741-2552/9/4/046006)

J. Neural Eng. **9** (2012) 046006 (13pp) doi:10.1088/1741-2560/9/4/046006

Accurate decoding of reaching movements from field potentials in the absence of spikes

Robert D Flint[1], **Eric W Lindberg**[1], **Luke R Jordan**[2], **Lee E Miller**[2,3,4,5] **and Marc W Slutzky**[1,2,3,5,6]

[1] Department of Neurology, Northwestern University, Chicago, IL 60611, USA
[2] Department of Physiology, Northwestern University, Chicago, IL 60611, USA
[3] Department of Physical Medicine and Rehabilitation, Northwestern University, Chicago, IL 60611, USA
[4] Department of Biomedical Engineering, Northwestern University, Chicago, IL 60611, USA
[5] Sensorimotor Performance Program, Rehabilitation Institute of Chicago, Chicago, IL 60611, USA

E-mail: mslutzky@northwestern.edu

Received 1 November 2011
Accepted for publication 16 May 2012
Published 25 June 2012
Online at stacks.iop.org/JNE/9/046006

Abstract
The recent explosion of interest in brain–machine interfaces (BMIs) has spurred research into choosing the optimal input signal source for a desired application. The signals with highest bandwidth—single neuron action potentials or spikes—typically are difficult to record for more than a few years after implantation of intracortical electrodes. Fortunately, field potentials recorded within the cortex (local field potentials, LFPs), at its surface (electrocorticograms, ECoG) and at the dural surface (epidural, EFPs) have also been shown to contain significant information about movement. However, the relative performance of these signals has not yet been directly compared. Furthermore, while it is widely postulated, it has not yet been demonstrated that these field potential signals are more durable than spike recordings. The aim of this study was to address both of these questions. We assessed the offline decoding performance of EFPs, LFPs and spikes, recorded sequentially, in primary motor cortex (M1) in terms of their ability to decode the target of reaching movements, as well as the endpoint trajectory. We also examined the decoding performance of LFPs on electrodes that are not recording spikes, compared with the performance when they did record spikes. Spikes were still present on some of the other electrodes throughout this study. We showed that LFPs performed nearly as well as spikes in decoding velocity, and slightly worse in decoding position and in target classification. EFP performance was slightly inferior to that reported for ECoG in humans. We also provided evidence demonstrating that movement-related information in the LFP remains high regardless of the ability to record spikes concurrently on the same electrodes. This is the first study to provide evidence that LFPs retain information about movement in the absence of spikes on the same electrodes. These results suggest that LFPs may indeed remain informative after spike recordings are lost, thereby providing a robust, accurate signal source for BMIs.

(Some figures may appear in colour only in the online journal)

[6] Author to whom any correspondence should be addressed.

Introduction

Movement-related information derived from spikes in the motor cortex (M1) has been used to control brain–machine interfaces (BMIs) that allow users to move a computer cursor [1–4] or a robotic arm [5], or to reanimate paralyzed muscles via functional electrical stimulation (FES [6–8]). However, with a few exceptions [9], multielectrode arrays typically lose most, if not all, of their spike signals within a few years of implantation.

Movement-related information also can be obtained from local field potentials, or LFPs [10–13], which represent the combined synaptic and dendritic activity from thousands of neurons [14–16]. There is uncertainty as to just how informative LFPs are relative to spikes, with some studies demonstrating less accuracy with LFPs [17–19] and others showing similar or greater accuracy [20–23].

Cortical surface potentials (electrocorticograms, ECoG) can also [24, 25] be used to decode reach target [21, 26] and kinematics of arm [27–31] and finger movements [32–34]. Mehring *et al* [35] found more information about movement in individual electrodes of monkey LFP than in individual electrodes of human ECoG. However, only one study [38] has compared extracortical and intracortical signals in the same animal performing the same task. While that study did find reach target decoding performance to be similar for intra and extracortical field potentials, it was performed in rats, which have much smaller anatomical features than monkeys or humans. Thus, results may differ in primates.

We showed previously that epidural recordings provide spatial resolution similar to ECoG [36]. Also, we [37, 38] and others [39] have demonstrated that epidural field potentials (EFPs) can be used to decode arm movement direction in both rats and monkeys. Others have demonstrated the feasibility of BMIs based on one [40, 41] or a few epidural electrodes [42, 43]. By preserving the integrity of the dura, epidural electrodes should offer lower risk of brain infection, subdural hemorrhage and stroke than subdural electrodes.

This study is the first ever to compare target and trajectory decoding using EFPs, LFPs and spikes recorded from the same brain areas of the same animals performing identical tasks. Using epidural signals, we were able to decode the target of reaching movements with accuracy similar to that reported for human ECoG. The relative accuracy of decoded endpoint trajectory was somewhat lower. In a separate set of experiments, we show that LFPs can be used to decode endpoint velocity with accuracy similar to that provided by spikes. Finally, while it is widely believed that field potentials might provide useful signals for longer durations than spikes, there is scant evidence of this to date. Our evidence that LFPs retain the same amount of information about movement, even when spike activity is absent from a given electrode, supports this idea.

Materials and methods

Behavior

All experiments were performed with approval from the Institutional Animal Care and Use Committee of Northwestern University. Two rhesus monkeys were trained to perform one of two reaching tasks while grasping a two-link manipulandum. The first was an eight-target, center-out task, with 2 cm square outer targets spaced at 45° intervals around a circle of radius 10 cm. Each trial began with the illumination of the target at the center of the circle. After a random hold time of 0.5–0.6 s, a randomly selected outer target was illuminated and the center target disappeared, signaling the monkey to start a reach. The monkey had to reach the outer target within 1.5 s and hold for a random time between 0.2 s and 0.4 s to obtain a liquid reward. The second task was a random-target task in which the monkey had to acquire a series of eight randomly positioned targets, holding in each for 0.1 s, to obtain the reward. The random-target task covered most of the endpoint kinematic state space and was used for all continuous decoding.

Electrode implantation and recording

We implanted monkey C with a custom-built, epidural microwire array over the proximal arm area of primary motor (M1) and premotor (PMd) cortices contralateral to the arm used to perform the task. This array consisted of an 8×8 grid of 50 μm microwires with 1 mm spacing, embedded in (and cut flush with) a Silastic mold. After several months of recordings, we removed this array and implanted a 96-channel silicon microelectrode array (Blackrock, Inc.) intracortically in the same area of M1 (figure 1). We implanted monkey M initially with an intracortical array in the arm area of M1, recorded for several months, then removed this array and implanted a 64-channel epidural array (split into two 4×8 halves) over the arm areas of M1 and PMd in the contralateral hemisphere. Monkey M performed the behavioral task with the arm contralateral to each recording array. Intracortical arrays were grounded to the Cereport pedestal and referenced to a platinum wire with 3 mm exposed wire length placed under the dura. Epidural arrays were grounded to a platinum wire with 3 mm exposed wire length and referenced to an extra electrode placed in the array.

Implant locations for intracortical arrays were confirmed by looking for movement elicited by intraoperative cortical surface stimulation using a monopolar, silver ball electrode with 2–5 mA, 200 μs pulses delivered at 60 Hz. Animals were anesthetized with inhaled isoflurane (2–3%), except during physiological testing, when reduced isoflurane (<0.5%) was supplemented with intravenous remifentanil to reduce suppression of cortical excitability. Anesthetic depth was assessed at all times by monitoring jaw muscle tone and vital signs. Surgical details are described in [44]. Stimulation using the same parameters was also performed through the implanted epidural electrode array in the laboratory in monkey C while sedated with ketamine.

We recorded both spikes and LFPs using a 128-channel acquisition system (Cerebus, Blackrock, Inc.) while the monkey performed the motor tasks. Spikes were obtained by sampling at 30 kHz, high-pass filtering at 300 Hz, thresholding and manually sorting offline. Thresholds were set manually for each channel, with an average level of 5.2 SD above the mean potential in each channel. Both single- and multi-unit spikes

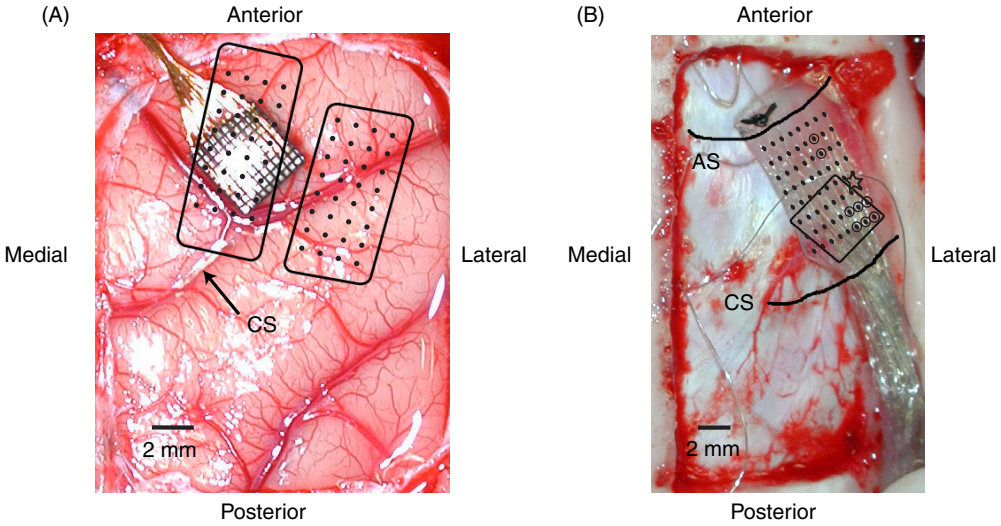

Figure 1. Positions of electrode arrays. (A) Monkey M's intracortical array and superimposed epidural arrays (which were implanted in the contralateral hemisphere) with approximate electrode positions noted as black dots. (B) Monkey C's epidural array, which was more anterior than monkey M's array, and approximate intracortical array location (square). Approximate locations of stimulation that caused hand and arm movement during surgery and during sedation in the laboratory are denoted by star and circles, respectively. CS, central sulcus; AS, arcuate sulcus. Scale bars represent 2 mm.

were used for all subsequent analyses. Field potentials (both LFPs and EFPs) were obtained by band-pass filtering between 0.5 and 500 Hz and sampling at 1 kHz for monkey M and 2 kHz for monkey C. Subsequently, the signals were digitally notch filtered at 120, 180 and 240 Hz to remove line noise. After epidural electrodes with obvious artifacts or clipping (determined both visually and aurally) were excluded from analysis, there remained 57 and 49 electrodes for monkeys C and M, respectively. For LFPs, two electrodes in each monkey's intracortical array were excluded from analysis due to significant noise. Multiple 10 min data files were recorded in each 60–90 min long experimental session. We recorded five and four sessions of EFPs from monkeys M and C, respectively, and four sessions of both LFPs and spikes from each monkey.

Discrete decoding: feature extraction, feature selection and decoder

We decoded the center-out reach target using at least 14 trials per reach direction. Spike signals were converted to firing rates in 100 ms bins. We extracted five features from each field potential signal: the local motor potential (LMP, [27]), defined as the moving average within a 256 ms window, and the power in four different frequency bands (0–4, 7–20, 70–200 and 200–300 Hz). We used the power in these bands relative to the power during the period from 2.0 to 1.5 s before movement onset. The power in each band was computed by applying fast Fourier transforms to 256 ms windows after applying a Hanning window. The windows were overlapped by 156 ms to provide a sample every 100 ms. The band power values (or spike firing rates) in seven time bins from 200 ms before to 500 ms after movement onset (as determined from the manipulandum's velocity) were used as features. This provided 35 features for each field potential electrode (3290 features total for 94 LFP electrodes; 1995 and 1715 features for EFP electrodes in monkeys C and M, respectively), and 7 for each spike signal. To reduce the dimensionality of the input space, a one-way ANOVA was calculated over all the trials for each feature across reach targets. For both field potentials and spikes, we selected the 40 features with lowest p-values (i.e. those that were most reliably related to reach target) to use in decoding each file. We chose to use 40 features based on the results of a feature-dropping curve from a file not used in the final analysis.

We applied linear discriminant analysis to these features and used ten-fold cross validation to quantify performance. The mean performance for each file was defined as the fraction of trials that were decoded correctly over all ten test folds.

Chance performance for the center-out task was estimated by randomly shuffling the target labels, and then performing the cross validation as above. This was repeated 100 times for each file, and the five highest accuracy values were averaged to estimate a 95% confidence interval for chance performance.

Continuous decoding: feature extraction, feature selection and decoder

We decoded the position and velocity of the manipulandum from 10 min data files collected during the random-target task. Spike signals from all single- and multi-unit recordings were converted to firing rates in 100 ms bins. We extracted six features from each field potential signal: the LMP and the power in five different frequency bands (0–4, 7–20, 70–115, 130–200 and 200–300 Hz), which were computed in the same manner as for discrete decoding. We computed the log of the power in each band relative to the log of the mean power in each band over the entire file, to provide a sample every 100 ms. We chose a subset of features for decoding using the absolute value of the correlation coefficient ($|r|$) between each feature and the recorded kinematics (endpoint position or velocity). The features were ranked in descending order of the mean of $|r|$ over both dimensions of the output, and the top 150 features

were used for decoding. We chose to use 150 features based on results of electrode-dropping curves, described below. We also computed the maximum, rather than the mean $|r|$, in case some features were highly correlated to only one dimension of movement. There was no substantial difference in performance between the two approaches.

We used a multiple-input, multiple-output Wiener cascade model [45] to decode the kinematic signals. This two-stage approach cascades a linear, dynamical subsystem with a static nonlinearity, and has been shown to improve decoding compared with linear Wiener filtering [44, 46]. In the first stage, a set of causal linear filters of 10 bin (1 s) length between the input features and outputs (position or velocity) was fit to a set of training data. In calculating the weights for the linear model, we used a ridge regression technique [47] to avoid ill-conditioned covariance matrices that otherwise result from the highly correlated inputs. The output of the Wiener filters was then convolved with a static nonlinearity [44] implemented by fitting a third-order polynomial between the Wiener filter output and the kinematic variables. Iteratively refitting the linear and nonlinear portions improved the fit by only 1%, and was therefore not pursued. Position and velocity were decoded independently from one another.

For each 10 min file, feature selection and training of the Wiener cascade decoder was performed using 9 min of data, then tested on the remaining minute of data. This was repeated ten times for each file, for ten-fold cross-validation. We calculated the mean coefficient of determination (r^2) between actual and decoded position or velocity over all folds in a file to represent performance for that file.

Chance performance in the random target task was estimated by implementing the Wiener cascade decoder on a phase-randomized version of the input signal, as in [48]. Briefly, we calculated the Fourier transform of the signal, randomized the phase component, reconstructed the signal by calculating the inverse Fourier transform, and calculated the coefficient of variation between the predicted and actual output signal as above. The process was repeated 100 times for each recording, and the five highest r^2 values were averaged to estimate a 95% confidence interval for chance decoding performance.

Feature contribution analysis

We used two methods to determine which features contributed most to the decoder output (and hence provided the most information about the movement). For discrete decoding, we computed two-dimensional histograms (summing across time bins and frequency bands) of the top N features used in each decoder (mean over all electrodes). For continuous decoding, we determined the relative contribution of spectral and temporal components in the top 150 features by calculating the following quantities [31]:

$$W_{\text{freq}} = \frac{\sum_{\text{elec}} \sum_{\text{time}} |w_{\text{freq,elec,time}}|}{\sum_{\text{freq}} \sum_{\text{elec}} \sum_{\text{time}} |w_{\text{freq,elec,time}}|},$$

$$W_{\text{time}} = \frac{\sum_{\text{freq}} \sum_{\text{elec}} |w_{\text{freq,elec,time}}|}{\sum_{\text{freq}} \sum_{\text{elec}} \sum_{\text{time}} |w_{\text{freq,elec,time}}|},$$

where $w_{\text{freq,elec,time}}$ is the filter weight for each electrode, frequency and time lag. W_{freq} and W_{time} provide measures of the relative contribution of each frequency band and time bin, respectively.

Electrode-dropping analysis

To estimate the optimal number of electrodes for continuous decoding, we generated electrode-dropping curves, similar to neuron-dropping curves [49]. After dropping each electrode, we recomputed the performance for the file. Electrodes were selected using the correlation coefficient method as described above, ranking electrodes by their mean $|r|$ over all frequency bands and dropping the least-informative electrodes. For LFPs and EFPs, all features associated with a given electrode were dropped together.

Analysis of LFP dependence on the presence of spikes

There is reason to be concerned that some of the information in the very high gamma bands (100–300 Hz) might be due directly to spiking activity. If this were true, then the information recorded in these bands might not have greater recording longevity than that of the spikes themselves. Therefore, we tested whether the performance of LFPs was dependent on the presence of spiking activity recorded at the same electrodes. If LFPs decode kinematics as accurately whether or not spikes were present, it would suggest that the information in LFPs is robust, and can be obtained independently of the ability to record spikes.

To test this, we identified pairs of files, each from different sessions, in which particular electrodes contained single- or multi-unit spikes in one but not the other session. We compared velocity decoding for the sessions with and without spikes using only the paired electrodes. To increase the number of session pairs used for comparisons, we performed the analysis both forward and backward in time, first using electrodes with spikes only in the earlier of two sessions, and then for electrodes that acquired spikes after an earlier session in which they were absent. These sessions were separated in time by at least one week and up to three weeks and nine months for monkeys M and C, respectively. Spikes were often present on other electrodes in the array at the times of recording these files, and sometimes returned on subsequent days in some of the paired electrodes used for LFP decoding.

Results

We recorded EFPs and intracortical LFPs and spikes sequentially from two monkeys during center-out and random-target experiments. We discriminated 74 $\pm$ 20 units and 119 $\pm$ 20 units (mean $\pm$ SD) per session for monkeys M and C, respectively. We analyzed EFPs and LFPs from 49 and 94 electrodes, respectively, in monkey M and 57 and 94 electrodes, respectively, in monkey C. To provide a sense of the relative power of the two types of field potentials, we examined the power spectra averaged over all electrodes for one file (figure 2(A)). Both types of field potentials peaked

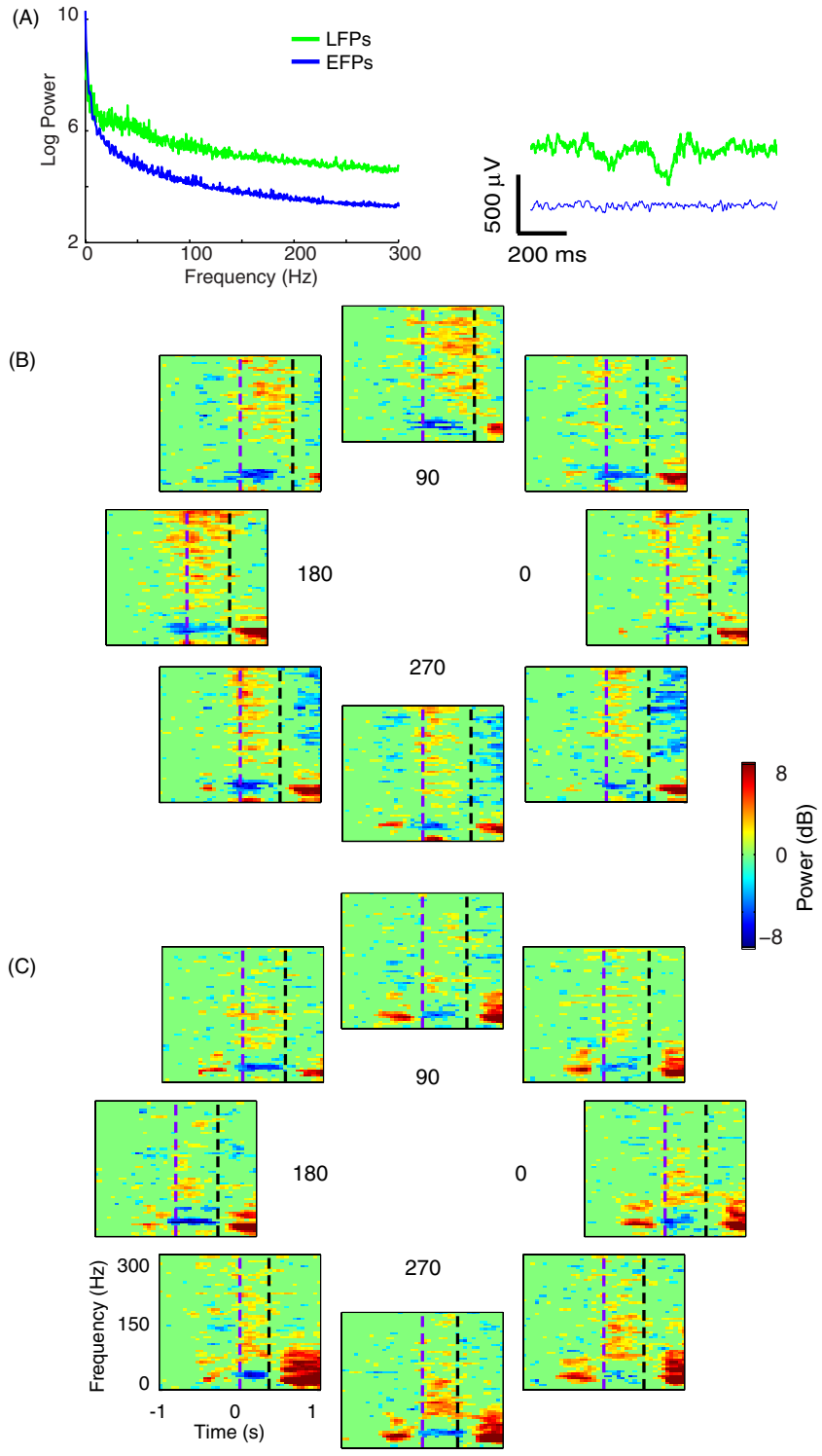

Figure 2. Frequency domain features of field potentials. (A) Mean power spectra of LFPs and EFPs over all electrodes in one file of data each, with examples of raw LFP and EFP on single channels (right). LFPs had substantially higher power in high-gamma bands than did EFPs. Despite this absolute power difference, ERSPs of single electrodes of (B) LFP and (C) EFP demonstrate that both EFPs and LFPs retain substantial relative power changes in delta (0–4 Hz), mu/beta (7–20 Hz) and high gamma (>70 Hz) from just prior to movement onset (first dashed line) to movement offset (second dashed line).

at very low frequencies, and exhibited approximate power-law scaling [50]. The power recorded by LFP electrodes was approximately 100 times greater than that recorded by EFP electrodes at most frequencies above ∼20 Hz, especially within the high-gamma (70–300 Hz) bands. Both LFPs (figure 2(B)) and EFPs (figure 2(C)) showed characteristic power decreases in mu (8–13 Hz) and beta (13–25 Hz) bands and power increases in high-gamma bands starting just before movement onset and ending after movement termination. These power changes tended to occur a bit sooner in LFPs

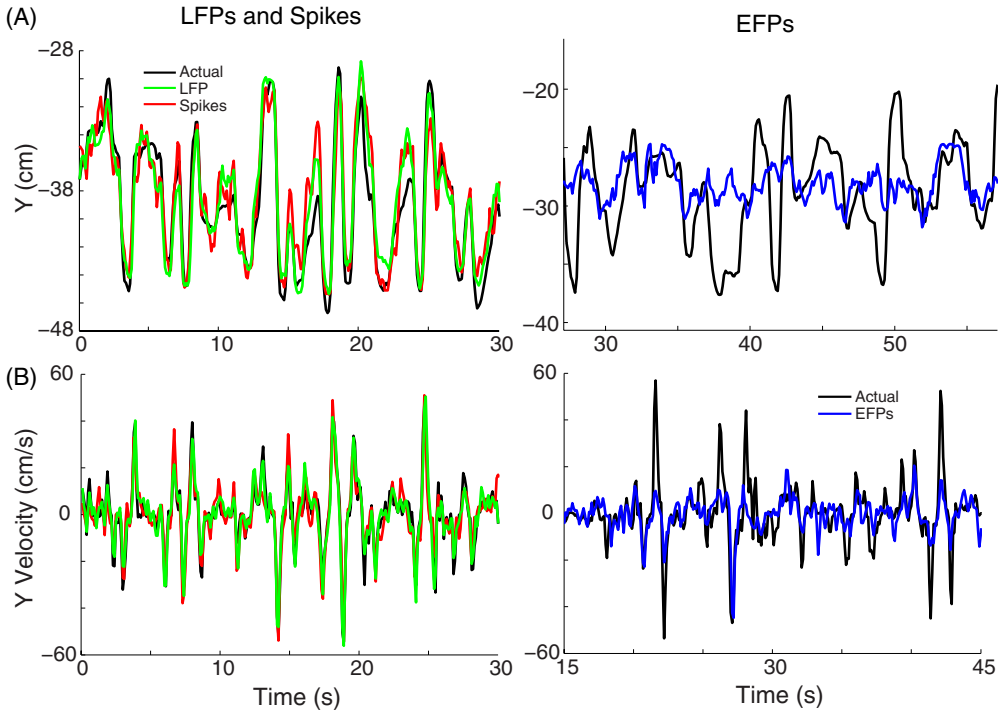

Figure 3. Examples of (A) position and (B) velocity decoding along the anterior–posterior (*Y*) axis using spikes, LFPs and EFPs. Decoding with spikes and LFPs provided close matches to the actual position and velocity (left panels). While EFPs (right panels) tended to decode the general direction of the movement correctly, they missed the peaks of the data.

than in EFPs. In these examples, the high-gamma band power was directionally tuned toward 180° in the LFP signal (figure 2(B)), and 270° in the EFP signal (figure 2(C)), showing the directional selectivity of these signals.

Continuous decoding

We decoded hand position and velocity offline from the random-target task, using 10 min data files. Spike and LFP data came from the same files, while EFP recordings were necessarily carried out in a different set of experiments. Figure 3 shows examples of position and velocity for the *Y* (anterior–posterior) axis decoded using each signal type. EFPs performed fairly well in estimating the direction of movement velocity, but the magnitude was inaccurate. In contrast, decoders using either LFPs or spikes predicted the trajectories very well. Figure 4 summarizes position and velocity decoding performance using all three signal types. In position decoding, EFPs ($r^2 = 0.08 \pm 0.03$ and 0.16 ± 0.10 for *X* and *Y* directions, respectively; $n = 10$ files in each monkey) were outperformed by LFPs ($r^2 = 0.55 \pm 0.08$ *X*, 0.68 ± 0.08 *Y*, $n = 8$ for each monkey), while spikes achieved the greatest decoding accuracy ($r^2 = 0.80 \pm 0.11$ *X*, 0.81 ± 0.08 *Y*, $n = 4$ for each monkey). These values were all higher than chance (95% confidence interval of $r^2 = 0.04$ for both *X* and *Y*). In velocity decoding, LFPs ($r^2 = 0.77 \pm 0.04$ *X*, 0.78 ± 0.05 *Y*) performed nearly identically to spikes ($r^2 = 0.77 \pm 0.08$ *X*, 0.79 ± 0.07 *Y*), while EFPs were dramatically outperformed by both ($r^2 = 0.09 \pm 0.05X$, 0.22 ± 0.08 *Y*), but were significantly higher than chance (95% confidence interval 0.02 for both *X* and *Y*). Decoding using EFPs, LFPs, and spikes underwent no significant change in performance over time (figure 4(C), $p > 0.14$ for all signal types, Pearson correlation test).

LFP decoding performance is independent of the presence of spikes

We sought to determine whether the ability to decode movements with LFPs was dependent on the presence of spike activity recorded concurrently on the same electrodes. We analyzed all paired combinations of four random-target files from each monkey, in which a subset of electrodes had spikes in one file but not in the other. These files were separated in time by at least one week and up to three weeks and nine months for monkeys M and C, respectively. We compared the LFP decoding performance (r^2) for files with concurrent spikes to the corresponding performance in the paired file without spikes. Spikes were present on some of the electrodes (including some of those used in LFP decoding, on subsequent days) throughout the study. The r^2 values from individual files ranged widely, as shown in figure 5. This wide variation was due mainly to the different numbers of electrodes used for decoding in different pairs of files, which ranged from 4 to 24. However, across all comparisons, the mean difference in r^2 for electrodes with and without spikes was not statistically significant (0.044 ± 0.13 and -0.003 ± 0.18 for *X* and *Y* velocities, respectively; mixed effects model, $p = 0.35$ and 0.31 for *X* and *Y*, respectively). Also, the same frequency bands contributed to decoders in electrodes whether

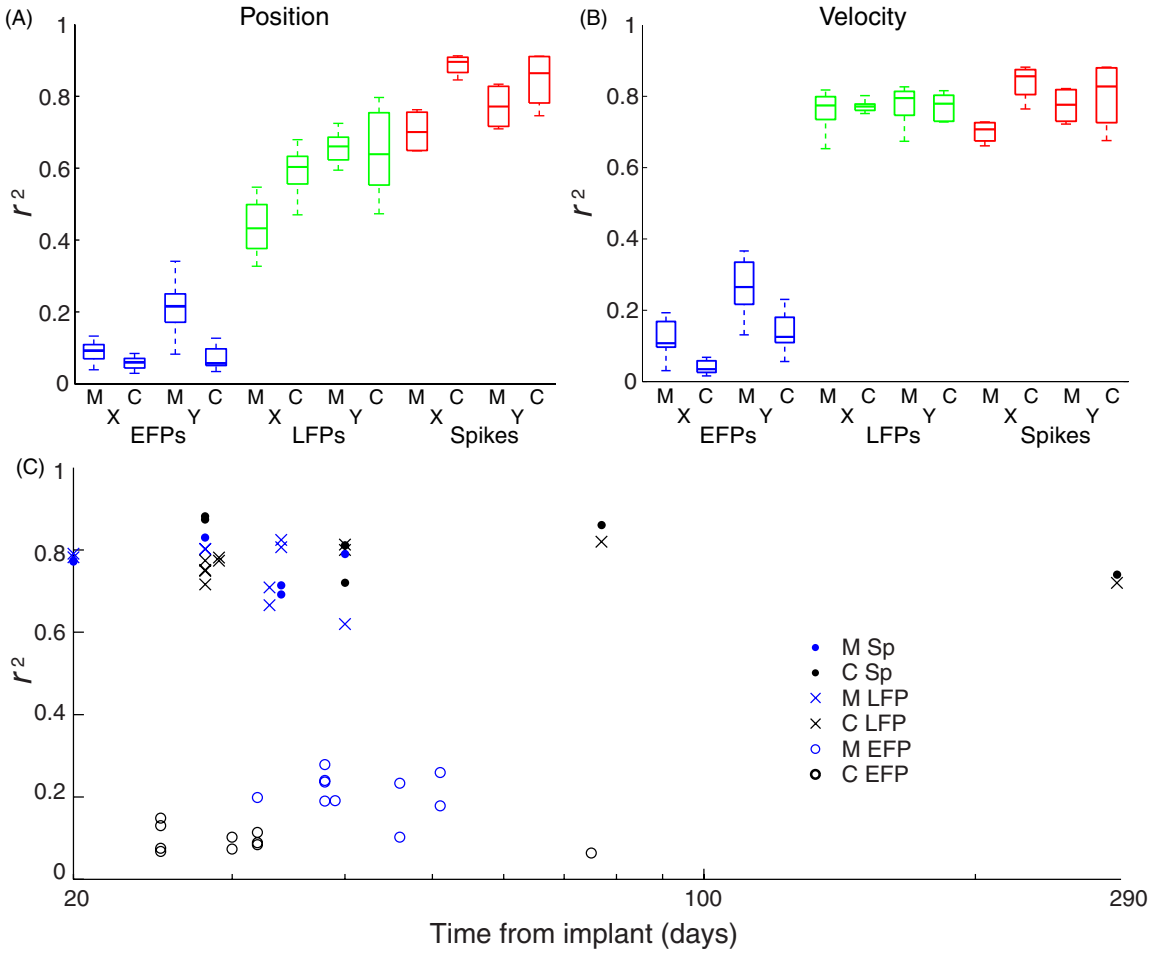

Figure 4. Continuous decoding performance in monkeys M and C for *X* and *Y* directions of (A) position and (B) velocity. Performance of LFPs was very similar to that of spikes in velocity estimation, somewhat worse in position estimation, while EFPs performed substantially poorer than either LFPs or spikes. (C) Velocity decoding performance for spikes (Sp), LFPs and EFPs over time.

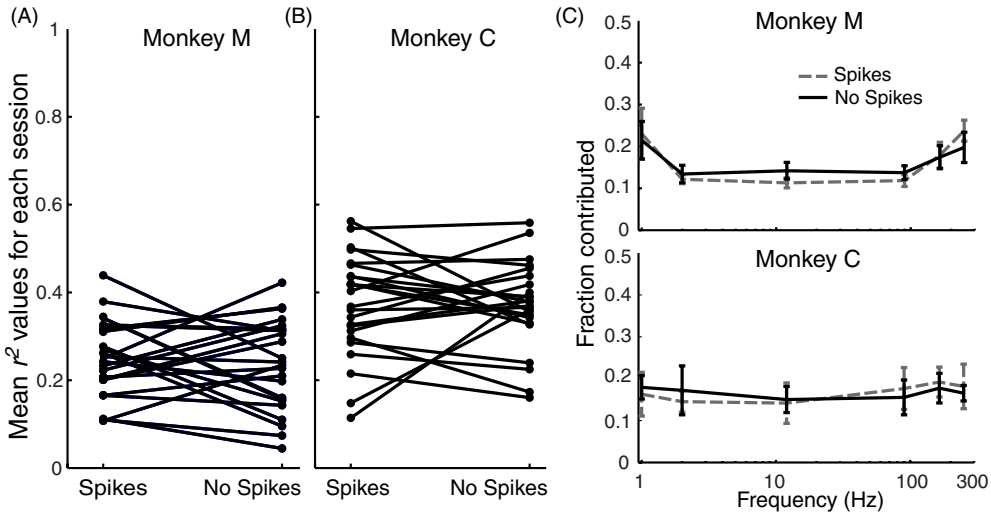

Figure 5. LFP decoding performance on electrodes in the presence or absence of spikes for (A) monkey M and (B) monkey C. Each dot represents the mean performance over ten folds of one file. Lines connect pairs of files using the same set of electrodes when spikes are present (Spike, left) and absent (No Spikes, right). (C) Contribution of frequency bands to the decoder was very similar for files with Spike (dashed lines) and No Spikes (solid lines) in both monkeys.

or not spikes were present. The high-gamma bands and LMP contributed most in both cases (figure 5(C)). The independence of LFP decoding accuracy from the presence or absence of concurrently recorded spikes on the same electrodes is the first direct evidence that LFPs can provide an accurate control signal even in the absence of spikes.

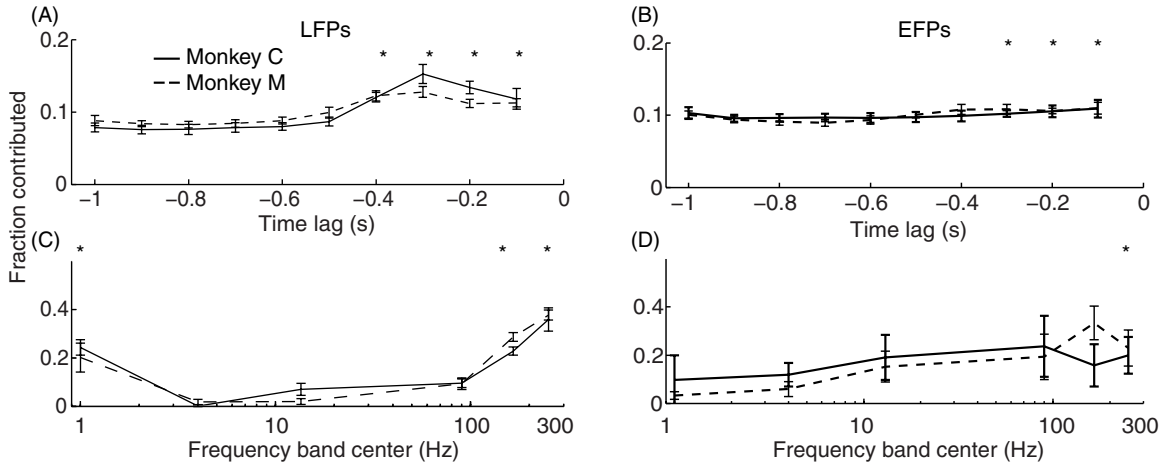

Figure 6. Feature contributions to velocity decoding (measured as fraction of total decoder weights) for both monkeys (C, solid lines, M, dashed lines). (A) and (B) Relative weight as a function of time lag using LFPs and EFPs, respectively. (C) and (D) Relative weights of frequency bands (plotted on a log scale at the midpoint of each band, with LMP and 0–4 Hz band plotted at 1 and 4 Hz, respectively, for clarity) using LFPs and EFPs, respectively. Error bars show standard deviations. Asterisks denote time bins or frequency bands which differed significantly from the median fraction over all bins/bands for both monkeys (Wilcoxon signed-rank test, $p < 0.05$).

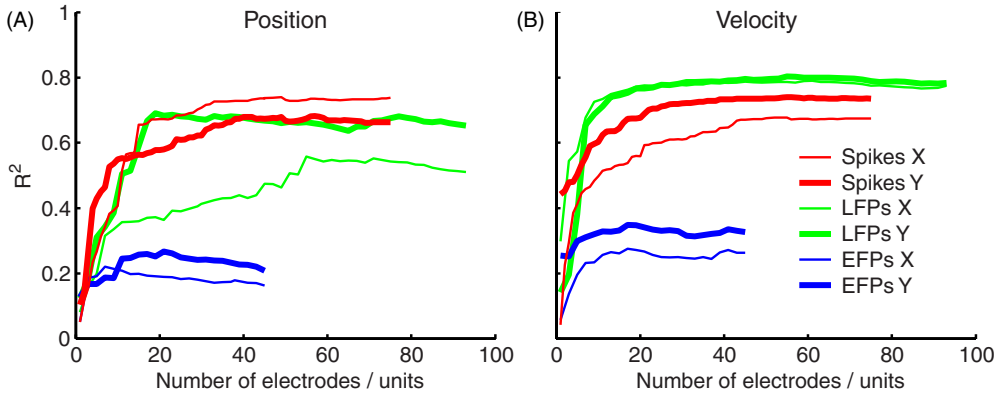

Figure 7. Dependence of decoding performance on number of electrodes (for field potentials) or units (for spikes). The features (inputs) that correlated least with the output were dropped first from decoding. (A) In position decoding, LFPs and spikes both reached a plateau between 20 and 40 electrodes or units, respectively. Performance was somewhat different for *X* and *Y* positions (thin and thick lines, respectively), especially for LFPs. For EFPs, decoding of both directions was similar and peaked by about 20 electrodes. These data are from one session with monkey M. (B) In velocity decoding, LFPs slightly outperformed spikes in this file. LFPs and EFPs reached maximum performance just before 20 electrodes.

Feature contribution to continuous decoding

The most informative time bins for LFPs were those from −300 to−200 ms, though bins from −400 to 0 ms contributed to the predictions (figure 6(A)). For EFPs, there was minimally more information in time bins from −200 to −100 ms (figure 6(B)). The LFP frequency features that contributed most to the decoders were the high-gamma bands, followed by the LMP (figure 6(C)). For EFPs, the difference between bands was less pronounced, though the high-gamma and mu/beta (7–20 Hz) bands tended to be more highly weighted for both monkeys (figure 6(D)). This suggests that there was more movement-related information in the highest frequency bands for intracortical signals than for EFPs.

We analyzed the effect on performance of the number of features with electrode- and neuron-dropping curves (figure 7). Both LFPs and EFPs reached peak performance with 20–30 electrodes (120–180 features) for velocity and slightly more features for position. Spike performance increased most rapidly in the first 20 units, but kept improving until about 60 units. These curves were largely consistent across files (not shown).

As prior studies showing that LFPs have high spatial correlation only examined the time domain or very low frequency band signal [17, 48], we also investigated the correlation between electrodes for each feature. We computed the correlation coefficients between all pairs of electrodes separately for each frequency band and LMP for the entire file duration. Figure 8 shows the mean correlations over all files for both monkeys combined. The LMP was most strongly correlated, especially for LFPs (figure 8(A)). For LFPs, the 0–4 Hz and 7–20 Hz bands were also highly correlated. EFPs were somewhat less correlated in LMP and low-frequency bands than LFPs (figure 8(B)). High-gamma bands had very low correlations for both LFPs and EFPs. Because this was also the same frequency range in which the LFP was maximally informative, it

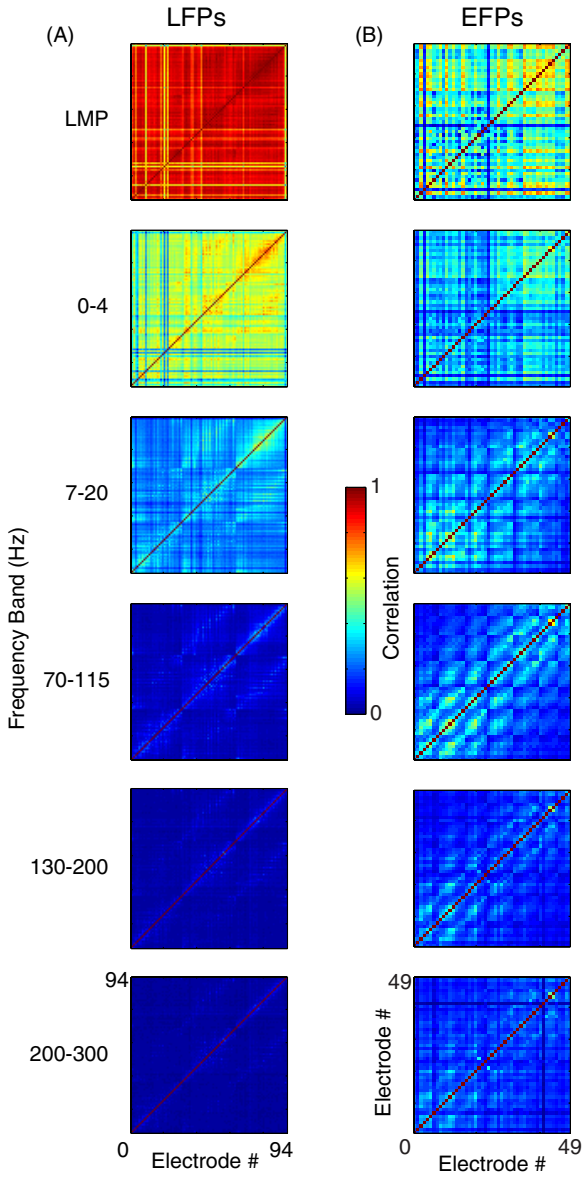

Figure 8. Cross correlation of frequency band power between electrode pairs for (A) LFPs and (B) EFPs. The LMP and lower frequency bands had the highest cross correlation for both EFPs and LFPs, especially for LFPs. High-gamma bands had very low correlations for LFPs, and slightly higher for EFPs.

suggests that these signals may be more highly localized than has been reported previously in studies using clinical ECoG arrays with 10 mm inter-electrode spacing [25, 34]. The same may also be true of the EFP signal, but this is more difficult to discern given its lower information content.

Discrete decoding

We decoded reach target direction offline from EFP signals, as well as from LFPs and spikes recorded during center-out experiments. Decoding performance using EFPs (0.35 $\pm$ 0.02 and 0.33 $\pm$ 0.02, mean $\pm$ SE, $n = 10$ files each for monkeys M and C, respectively) was significantly better than chance (95% confidence interval of 0.14) and similar to that reported in the literature for subdural signals. Performance improved when using LFPs (0.54 $\pm$ 0.02 and 0.58 $\pm$ 0.04, $n = 8$, monkeys M and C, respectively), but both types of field potentials were substantially outperformed by decoding from spikes (0.81 $\pm$ 0.02 and 0.92 $\pm$ 0.02, $n = 6$ and 4, monkeys M and C, respectively). These data are summarized in figure 9(A). The mean ($\pm$ SD) number of trials in each file was 146 $\pm$ 36; performance did not change within this range of trials. Classification errors using spike and LFP inputs were more likely to include nearby targets, as seen in the confusion matrices (figure 9(B)). The percentage of targets that were identified correctly or within one target of the correct one was 99% for spikes, 86% for LFPs and 58% for EFPs.

Feature contribution to discrete decoding

The features contributing the most to discrete decoding using LFPs and EFPs are shown in figure 9(C). The high-gamma bands were most important in LFPs, with a second peak in the 0–4 Hz band around movement onset. Decoding with EFPs also showed a peak in the 0–4 Hz band around movement onset, though overall a wider range of features was used.

Discussion

In this study, we have demonstrated that LFPs contain almost as much information about reach velocity as do spikes, and substantial information about reach position. Furthermore, we showed that LFPs contain information that persists despite the absence of simultaneously recorded spikes. These findings represent good evidence that field potentials could provide a high-quality signal source that is more robust than spikes for chronic recordings. In addition, this is the first study to compare performance of EFPs directly with that of intracortical LFPs and spikes recorded from the same areas of cortex in the same animals performing identical behavioral tasks. EFPs were used to decode reach target with accuracy inferior to LFPs. LFPs and spikes greatly outperformed EFPs in kinematic trajectory decoding. Velocity decoding using EFPs was only slightly inferior to that using subdural signals in humans [27–29, 51]. This leads us to conclude that there is a considerably greater information difference between intra- and extra-cortical signals than between subdural and epidural signals.

LFPs contain almost as much information about kinematics as do spikes

Velocity-decoding performance using LFPs rivaled that using spikes from the same files. Prior studies of kinematic decoding using M1 LFPs reported r values ranging from 0.60 to 0.74 [17, 18] for position, and 0.5 to 0.7 for velocity ([18], using only single-frequency bands), while performance using M1 spikes ranged from 0.72 to 0.90 [3, 49, 52]. Our results suggest that even higher velocity decoding performance using LFPs can be achieved ($r^2 = 0.78$, corresponding to $r \sim 0.9$). Position decoding using LFPs in our study was slightly worse; this was also seen in [48]. Target decoding using LFPs also was inferior to spikes, but compares favorably with prior LFP studies

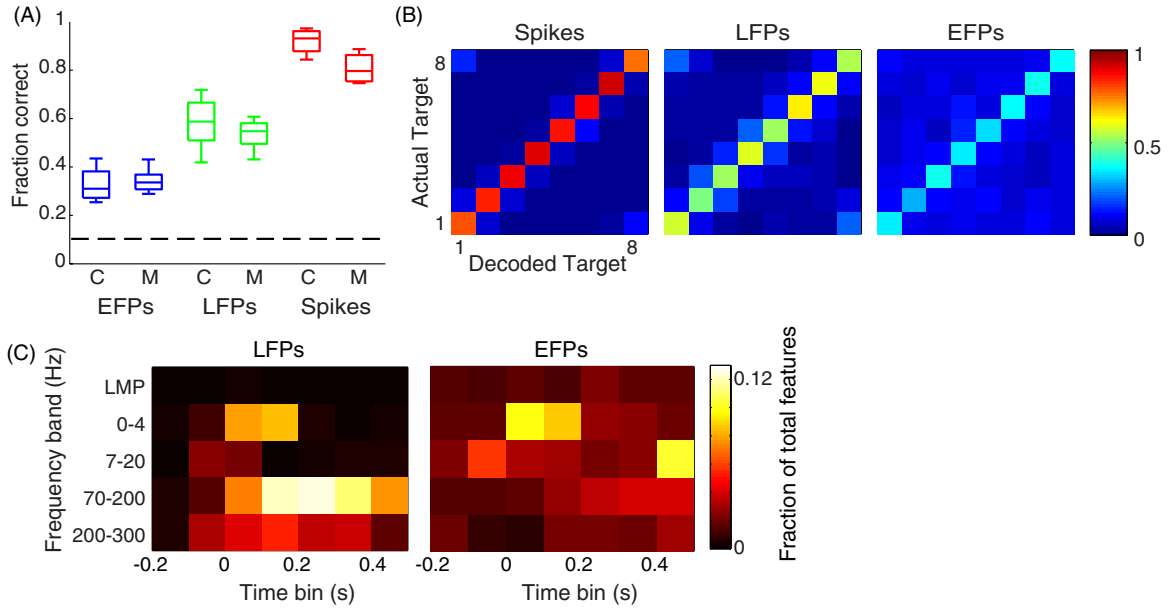

Figure 9. (A) Target decoding results for spikes, LFPs and EFPs for both monkeys (C and M). Field potentials were decoded using all frequency bands. Dashed line represents chance performance determined empirically (14%). (B) Confusion matrices for EFPs, LFPs and spikes averaged over all files in both monkeys. Color represents the fraction of decoded targets classified for each actual target. (C) Histogram of features used in target decoding with LFPs and EFPs. The high-gamma bands were used most with LFPs, while the 0–4 Hz band was used most in EFPs. Time bins at and shortly after movement onset were most highly weighted in both LFPs and EFPs.

in monkeys, for which accuracies ranged from 0.45 to 0.87 [13, 17, 21], though the highest value represented data pooled from multiple files [21]. LFP performance saturated with more than 20 inputs, and actually exceeded spike performance when there were fewer than 50 inputs. This agrees with previous studies showing higher performance with LFPs compared to spikes for small numbers of inputs [21, 48]. Finally, we performed all decoding analyses offline, and it is possible that performance could be improved with online BMI use, as the brain adapts to the BMI [53].

LFP decoding performance was independent of spike presence

LFP decoding performance was not diminished when discriminable spike activity was absent. This suggests that field potential recordings may serve as a source of movement-related information that persists longer than spike recordings. Although this is widely postulated to be the case [54], there currently exists little evidence. Simeral *et al* [9] demonstrated that beta desynchronization with attempted movement remained at 1000 days after implantation in a paralyzed human subject even on channels that had lost all spike signals. However, they did not report whether high-gamma power increases remained, or whether LFPs retained sufficient information to decode attempted movements or to control a BMI. We compared pairs of files both forward and backward in time, and sometimes spikes reappeared on some channels that had lost them for a time; thus our results do not fully approximate the process of spike loss over time. Nevertheless, our results indicate that field potentials do indeed retain sufficient information to decode movement in the absence of spikes on the same electrodes.

The precise physiological relationship between spikes and LFPs is still uncertain. The current understanding is that LFPs originate from post-synaptic potentials [14, 55] and local processing activity [56, 57]. Several studies have found evidence that information in spikes is related to the high-gamma [57–61] or delta bands of LFPs [48]. Our results complement these studies by showing that LFPs contain only slightly less information about movement than do spikes. Since the high-gamma band was the most predictive component in our LFP decoders, it might provide a highly informative replacement for, or supplement to, spikes in neuroprostheses or chronic experiments. Moreover, the fact that the high-gamma band contributed most to decoders regardless of the presence or absence of spikes provides evidence that this band is not merely low-pass filtered spiking activity.

Epidural signals may provide a viable, minimally invasive signal source for BMIs

This study demonstrates that epidural signals can provide substantial information about reach target, though less about reach trajectory, and not nearly as much as intracortical signals. Overall, the reach target decoding results using EFPs presented here are similar to performance using either EFPs in rats [38] or ECoG in humans [26, 35]. Our trajectory decoding performance using EFPs was slightly inferior to the performance of subdural arrays in humans [27, 29] and epidural electrodes in monkeys ($r \sim 0.5$), and substantially inferior to that reported using subdural electrodes in monkeys ($r \sim 0.7$, [31]). These results complement other studies that demonstrated BMIs using a few EFPs allowed both humans [40] and non-human primates [42, 43] to control a cursor in two dimensions.

However, it is difficult to make comparisons between our results and other studies due to the substantially different methods (numbers of targets; electrode size, spacing, and number; behavioral task; species and decoding algorithms). For example, the EFP electrodes used in this study were only 50 μm in diameter, with significantly higher impedances (∼200 kΩ on average), and perhaps lower signal-to-noise ratios, than the much larger contacts (2–3 mm diameter) used in most human [26, 27, 29, 35] and monkey studies [31]. The optimal size of electrode contacts for decoding from surface recordings is not yet determined, so this may account for some differences between studies.

Ultimately, while EFPs were outperformed by intracortical signals, they are significantly less invasive, and may suffice for simpler BMI applications such as target selection. Developing a range of signal sources for BMIs may provide clinicians with better opportunities to match a neural prosthetic to each patient based on functional requirements and safety profile. Thus, we believe EFPs warrant further investigation as BMI inputs.

Time and frequency information

The most information about movement was obtained from the bin centered at −170 ms for both LFPs and EFPs. This is close to estimates of the optimal time lag between spike discharge and velocity, which have ranged from −100 to −122 ms [62–64].

The high-gamma band was the most informative for LFP signals, followed by the LMP. This agrees with prior studies showing greater kinematic information in high-gamma than in other frequency bands [18]. While it is unclear whether subsets of this band represent distinctly different information [28, 65] or are part of a broadband power change [50, 66], it is at least clear that there is a great deal of information in the 70–300 Hz range. For EFPs, high-gamma and mu/beta bands were most informative in trajectory decoding, while delta band was most informative in reach target decoding. Thus, high-gamma information appeared to diminish between intracortical and epidural electrodes, which could be due to global attenuation of an already small signal (figure 2(B)) by volume conduction through the intervening tissues [67].

Prior studies suggesting that LFPs were highly correlated [48] across distances of 1 cm [17] primarily examined time-domain LFP signals. Other studies have shown that movement-related activity in the LMP and mu/beta bands of ECoG is distributed broadly over the cortex, while the high-gamma features reflect more focal activity [25, 34], although one study using LFPs [68] showed synchronous activity in 20–80 Hz oscillations at sites up to 5 mm apart. Our results from cross-correlation analysis corroborate and extend these findings by showing little correlation for high-gamma features at even smaller spatial scales both intracortically (0.4 mm) and epidurally (1 mm). Thus, high-gamma oscillations, particularly in LFPs, are both highly informative and well localized, which makes them important alternatives to spikes in BMIs and for studying brain physiology with chronic electrode implants.

Implications for BMIs

The results presented here show that local field potentials can decode velocity with nearly the same accuracy as spikes, and likely with greater longevity. While it is very possible (though unproven) that multi-unit activity [17] may also retain information without the presence of single-unit spikes, recording such activity may require high-bandwidth sampling (∼30 kHz) as opposed to the much lower bandwidth (1 kHz) necessary for field potentials. Higher bandwidth translates into higher power requirements and thus increased heat and size of a potential prosthesis. Minimizing these factors may be critical in designing a clinically viable device. Thus, local field potentials could provide a signal source for brain–machine interfaces that optimizes the combination of information, longevity and narrow bandwidth.

Acknowledgments

This work was supported by NIH grants K08NS060223 and R01NS048845. The authors would like to thank Nicholas Hatsopoulos, Brian London and Christian Ethier for surgical assistance, Eric Perreault for computational assistance, and Mary Kwasny for statistical assistance.

References

[1] Serruya M D, Hatsopoulos N G, Paninski L, Fellows M R and Donoghue J P 2002 Instant neural control of a movement signal *Nature* **416** 141–2

[2] Taylor D M, Tillery S I and Schwartz A B 2002 Direct cortical control of 3D neuroprosthetic devices *Science* **296** 1829–32

[3] Carmena J M, Lebedev M A, Crist R E, O'Doherty J E, Santucci D M, Dimitrov D F, Patil P G, Henriquez C S and Nicolelis M A 2003 Learning to control a brain-machine interface for reaching and grasping by primates *PLoS Biol.* **1** E42

[4] Hochberg L R, Serruya M D, Friehs G M, Mukand J A, Saleh M, Caplan A H, Branner A, Chen D, Penn R D and Donoghue J P 2006 Neuronal ensemble control of prosthetic devices by a human with tetraplegia *Nature* **442** 164–71

[5] Velliste M, Perel S, Spalding M C, Whitford A S and Schwartz A B 2008 Cortical control of a prosthetic arm for self-feeding *Nature* **453** 1098–101

[6] Pohlmeyer E A, Perreault E J, Slutzky M W, Kilgore K L, Kirsch R F, Taylor D M and Miller L E 2007 Use of intracortical recordings to control a hand neuroprosthesis *Proc. IEEE/EMBS Conf. Neural Eng.* pp 418–20

[7] Moritz C T, Perlmutter S I and Fetz E E 2008 Direct control of paralysed muscles by cortical neurons *Nature* **456** 639–42

[8] Oby E R, Ethier C, Bauman M J, Perreault E J, Ko J and Miller L E 2010 *Statistical Signal Processing for Neuroscience and Neurotechnology* ed K G Oweiss (New York: Academic, Elsevier) pp 369–406

[9] Simeral J D, Kim S P, Black M J, Donoghue J P and Hochberg L R 2011 Neural control of cursor trajectory and click by a human with tetraplegia 1000 days after implant of an intracortical microelectrode array *J. Neural Eng.* **8** 025027

[10] Sanes J N and Donoghue J P 1993 Oscillations in local field potentials of the primate motor cortex during voluntary movement *Proc. Natl Acad. Sci.* **90** 4470

[11] Murthy V N and Fetz E E 1996 Oscillatory activity in sensorimotor cortex of awake monkeys: synchronization of

local field potentials and relation to behavior *J. Neurophysiol.* **76** 3949

[12] Heldman D A, Wang W, Chan S S and Moran D W 2006 Local field potential spectral tuning in motor cortex during reaching *IEEE Trans. Neural Syst. Rehabil. Eng.* **14** 180–3

[13] O'Leary J G and Hatsopoulos N G 2006 Early visuomotor representations revealed from evoked local field potentials in motor and premotor cortical areas *J. Neurophysiol.* **96** 1492

[14] Mitzdorf U 1985 Current source-density method and application in cat cerebral cortex: investigation of evoked potentials and EEG phenomena *Physiol. Rev.* **65** 37

[15] Pesaran B 2009 Uncovering the mysterious origins of local field potentials *Neuron* **61** 1–2

[16] Logothetis N K 2003 The underpinnings of the BOLD functional magnetic resonance imaging signal *J. Neurosci.* **23** 3963

[17] Stark E and Abeles M 2007 Predicting movement from multiunit activity *J. Neurosci.* **27** 8387–94

[18] Zhuang J, Truccolo W, Vargas-Irwin C and Donoghue J P 2010 Decoding 3-D reach and grasp kinematics from high-frequency local field potentials in primate primary motor cortex *IEEE Trans. Biomed. Eng.* **57** 1774–84

[19] Bansal A K, Truccolo W, Vargas-Irwin C E and Donoghue J P 2011 Decoding 3-D reach and grasp from hybrid signals in motor and premotor cortices: spikes, multiunit activity and local field potentials *J. Neurophysiol.* **107** 1337–55

[20] Pesaran B, Pezaris J S, Sahani M, Mitra P P and Andersen R A 2002 Temporal structure in neuronal activity during working memory in macaque parietal cortex *Nature Neurosci.* **5** 805–114

[21] Mehring C, Rickert J, Vaadia E, Cardosa de Oliveira S, Aertsen A and Rotter S 2003 Inference of hand movements from local field potentials in monkey motor cortex *Nature Neurosci.* **6** 1253–4

[22] Scherberger H, Jarvis M R and Andersen R A 2005 Cortical local field potential encodes movement intentions in the posterior parietal cortex *Neuron* **46** 347–54

[23] Flint R D, Ethier C, Oby E R, Miller L E and Slutzky M W 2012 Local field potentials allow accurate decoding of muscle activity *J. Neurophysiol.* doi:10.1152/jn.00832.2011

[24] Crone N E, Miglioretti D L, Gordon B and Lesser R P 1998 Functional mapping of human sensorimotor cortex with electrocorticographic spectral analysis: II. Event-related synchronization in the gamma band *Brain* **121** 2301–15

[25] Miller K J, Leuthardt E C, Schalk G, Rao R P, Anderson N R, Moran D W, Miller J W and Ojemann J G 2007 Spectral changes in cortical surface potentials during motor movement *J. Neurosci.* **27** 2424–32

[26] Ball T, Schulze-Bonhage A, Aertsen A and Mehring C 2009 Differential representation of arm movement direction in relation to cortical anatomy and function *J. Neural Eng.* **6** 016006

[27] Schalk G, Kubanek J, Miller K J, Anderson N R, Leuthardt E C, Ojemann J G, Limbrick D, Moran D, Gerhardt L A and Wolpaw J R 2007 Decoding two-dimensional movement trajectories using electrocorticographic signals in humans *J. Neural Eng.* **4** 264–75

[28] Sanchez J C, Gunduz A, Carney P R and Principe J C 2008 Extraction and localization of mesoscopic motor control signals for human ECoG neuroprosthetics *J. Neurosci. Methods* **167** 63–81

[29] Pistohl T, Ball T, Schulze-Bonhage A, Aertsen A and Mehring C 2008 Prediction of arm movement trajectories from ECoG-recordings in humans *J. Neurosci. Methods* **167** 105–14

[30] Ganguly K, Secundo L, Ranade G, Orsborn A, Chang E F, Dimitrov D F, Wallis J D, Barbaro N M, Knight R T and Carmena J M 2009 Cortical representation of ipsilateral arm movements in monkey and man *J. Neurosci.* **29** 12948

[31] Chao Z C, Nagasaka Y and Fujii N 2010 Long-term asynchronous decoding of arm motion using electrocorticographic signals in monkeys *Front. Neuroeng.* **3** 3 (doi:10.3389/fneng.2010.00003)

[32] Acharya S, Fifer M S, Benz H L, Crone N E and Thakor N V 2010 Electrocorticographic amplitude predicts finger positions during slow grasping motions of the hand *J. Neural Eng.* **7** 046002

[33] Miller K J, Zanos S, Fetz E E, den Nijs M and Ojemann J G 2009 Decoupling the cortical power spectrum reveals real-time representation of individual finger movements in humans *J. Neurosci.* **29** 3132–7

[34] Kubanek J, Miller K J, Ojemann J G, Wolpaw J R and Schalk G 2009 Decoding flexion of individual fingers using electrocorticographic signals in humans *J. Neural Eng.* **6** 066001

[35] Mehring C, Nawrot M P, de Oliveira S C, Vaadia E, Schulze-Bonhage A, Aertsen A and Ball T 2004 Comparing information about arm movement direction in single channels of local and epicortical field potentials from monkey and human motor cortex *J. Physiol. Paris* **98** 498–506

[36] Slutzky M W, Jordan L R, Krieg T, Chen M, Mogul D J and Miller L E 2010 Optimal spacing of surface electrode arrays for brain-machine interface applications *J. Neural Eng.* **7** 026004

[37] Slutzky M W, Jordan L R and Miller L E 2009 Evaluation of epidural and intracortical field potentials as control inputs for brain-machine interfaces *Society of Neuroscience Annu. Meeting*

[38] Slutzky M W, Jordan L R, Lindberg E W, Lindsay K E and Miller L E 2011 Decoding the rat forelimb movement direction from epidural and intracortical field potentials *J. Neural Eng.* **8** 036013

[39] Shimoda K, Chao Z C, Nagasaka Y and Fujii N 2010 Decoding continuous 3D hand trajectories from epidural electrocorticography in Japanese macaque *Society of Neuroscience Annu. Meeting*

[40] Leuthardt E C, Miller K J, Schalk G, Rao R P and Ojemann J G 2006 Electrocorticography-based brain computer interface—the Seattle experience *IEEE Trans. Neural Syst. Rehabil. Eng.* **14** 194–8

[41] Kennedy P, Andreasen D, Ehirim P, King B, Kirby T, Mao H and Moore M 2004 Using human extra-cortical local field potentials to control a switch *J. Neural Eng.* **1** 72–7

[42] Rouse A G, Heldman D A and Moran D W 2007 Neural adaptation of epidural electrocorticographic (EECoG) signals during closed-loop brain computer interface (BCI) control *Society of Neuroscience Annu. Meeting*

[43] Rouse A G, Williams J J, Wheeler J J and Moran D 2010 The effect of electrode distance and neural plasticity on an epidural electrocorticographic (EECoG) closed-loop brain-computer interface (BCI) *Society of Neuroscience Annu. Meeting*

[44] Pohlmeyer E A, Solla S A, Perreault E J and Miller L E 2007 Prediction of upper limb muscle activity from motor cortical discharge during reaching *J. Neural Eng.* **4** 11

[45] Hunter I W and Korenberg M J 1986 The identification of nonlinear biological systems: Wiener and Hammerstein cascade models *Biol. Cybern.* **55** 135–44

[46] Perreault E J, Kirsch R F and Acosta A M 1999 Multiple-input, multiple-output system identification for characterization of limb stiffness dynamics *Biol. Cybern.* **80** 327–37

[47] Nemati S, Fagg A H, Hatsopoulos N G and Miller L E 2007 A comparison of linear and kalman filter models for arm motion prediction *Proc. Annu. Meeting of the Neural Control of Movement*

[48] Bansal A K, Vargas-Irwin C E, Truccolo W and Donoghue J P 2011 Relationships among low-frequency local field potentials, spiking activity, and three-dimensional reach and grasp kinematics in primary motor and ventral premotor cortices *J. Neurophysiol.* **105** 1603–19

[49] Wessberg J, Stambaugh C R, Kralik J D, Beck P D, Laubach M, Chapin J K, Kim J, Biggs S J, Srinivasan M A and Nicolelis M A 2000 Real-time prediction of hand trajectory by ensembles of cortical neurons in primates *Nature* **408** 361–5

[50] Miller K J, Sorensen L B, Ojemann J G and den Nijs M 2009 Power-law scaling in the brain surface electric potential *PLoS Comput. Biol.* **5** e1000609

[51] Rickert J, Oliveira S C, Vaadia E, Aertsen A, Rotter S and Mehring C 2005 Encoding of movement direction in different frequency ranges of motor cortical local field potentials *J. Neurosci.* **25** 8815–24

[52] Wu W, Gao Y, Bienenstock E, Donoghue J P and Black M J 2006 Bayesian population decoding of motor cortical activity using a Kalman filter *Neural Comput.* **18** 80–118

[53] Ganguly K and Carmena J M 2009 Emergence of a stable cortical map for neuroprosthetic control *PLoS Biol.* **7** e1000153

[54] Andersen R A, Musallam S and Pesaran B 2004 Selecting the signals for a brain-machine interface *Curr. Opin. Neurobiol.* **14** 720–6

[55] Bartos M, Vida I and Jonas P 2007 Synaptic mechanisms of synchronized gamma oscillations in inhibitory interneuron networks *Nature Rev. Neurosci.* **8** 45–56

[56] Kamondi A, Acsady L, Wang X J and Buzsaki G 1998 Theta oscillations in somata and dendrites of hippocampal pyramidal cells *in vivo*: activity-dependent phase-precession of action potentials *Hippocampus* **8** 244–61

[57] Rasch M J, Gretton A, Murayama Y, Maass W and Logothetis N K 2008 Inferring spike trains from local field potentials *J. Neurophysiol.* **99** 1461–76

[58] Csicsvari J, Jamieson B, Wise K D and Buzsaki G 2003 Mechanisms of gamma oscillations in the hippocampus of the behaving rat *Neuron* **37** 311–22

[59] Jacobs J, Kahana M J, Ekstrom A D and Fried I 2007 Brain oscillations control timing of single-neuron activity in humans *J. Neurosci.* **27** 3839–44

[60] Ray S, Crone N E, Niebur E, Franaszczuk P J and Hsiao S S 2008 Neural correlates of high-gamma oscillations (60–200 Hz) in macaque local field potentials and their potential implications in electrocorticography *J. Neurosci.* **28** 11526–36

[61] Whittingstall K and Logothetis N K 2009 Frequency-band coupling in surface EEG reflects spiking activity in monkey visual cortex *Neuron* **64** 281–9

[62] Moran D W and Schwartz A B 1999 Motor cortical representation of speed and direction during reaching *J. Neurophysiol.* **82** 2676–92

[63] Paninski L, Fellows M R, Hatsopoulos N G and Donoghue J P 2004 Spatiotemporal tuning of motor cortical neurons for hand position and velocity *J. Neurophysiol.* **91** 515–32

[64] Wang W, Chan S S, Heldman D A and Moran D W 2007 Motor cortical representation of position and velocity during reaching *J. Neurophysiol.* **97** 4258

[65] Gaona C M, Sharma M, Freudenburg Z V, Breshears J D, Bundy D T, Roland J, Barbour D L, Schalk G and Leuthardt E C 2011 Nonuniform High-Gamma (60–500 Hz) power changes dissociate cognitive task and anatomy in human cortex *J. Neurosci.* **31** 2091–100

[66] Manning J R, Jacobs J, Fried I and Kahana M J 2009 Broadband shifts in local field potential power spectra are correlated with single-neuron spiking in humans *J. Neurosci.* **29** 13613–20

[67] Nunez P L and Srinivasan R 2006 *Electric Fields of the Brain: The Neurophysics of EEG* (New York: Oxford University Press)

[68] Donoghue J P, Sanes J N, Hatsopoulos N G and Gaal G 1998 Neural discharge and local field potential oscillations in primate motor cortex during voluntary movements *J. Neurophysiol.* **79** 159–73